Contribution from the Departments of Chemistry, University of Notre Dame, Notre Dame, Indiana 46556, and Southern Methodist University, Dallas, Texas 75275

Quantum-Chemical Investigation of $(2,2'\text{-bpy})SnB_4H_4(CCH_3)_2$ and $(CO)_3FeB_4H_4(CCH_3)_2$. Origin of Observed Structural Distortions from Idealized Closo Geometries

Reynaldo D. Barreto,[†] Thomas P. Fehlner,*[†] and Narayan S. Hosmane[‡]

Received August 13, 1987

Structural distortions from an idealized closo geometry in main-group- and transition-metal carborane clusters are examined by using the Fenske–Hall quantum-chemical technique. Experimentally, derivatives of $(2,2'\text{-bpy})SnB_4H_4(CCH_3)_2$ exhibit a metal center that is slipped toward the unique boron on the open B_3C_2 face of the carborane fragment while the opposite is true for $(CO)_3FeB_4H_4(CCH_3)_2$. MO calculations on the slipped geometries were compared with those of hypothetical structures having the main group or transition metal centered over the B_3C_2 face. The distortion in the tin system is principally caused by the necessity to relieve an antibonding interaction between a metal "lone pair" and the cage carbons of the carborane fragment. In the Fe system, this antibonding interaction exists between the "t_{2g}" metal set and the cage carbons but is very weak. Hence, normal cluster-bonding effects lead to the observed structure.

Introduction

The study of boranes and carboranes constitutes a mature subdiscipline of inorganic chemistry in that a wide range of compounds have been characterized both experimentally and theoretically.[1] Related systems containing main-group metals and transition metals have also been extensively studied.[2,3] Although such systems are analogous to boranes or carboranes, they can exhibit significantly different structures because of the unique characteristics of the metal fragments.[4] Mononuclear metallacarboranes containing the fragments $B_9H_{11-n}C_2R_n^{2-}$ and $B_4H_{6-n}C_2R_n^{2-}$ (n = 0–2, R = substituent) are well-documented in a structural sense. In these clusters, the metal caps the open B_3C_2 face of the nido carborane. However, the structures of these species sometimes deviate significantly from an idealized closo deltahedron in that the metal fragment is not found on the centroid of the B_3C_2 face but rather slipped toward or away from the unique boron. The direction and magnitude of this distortion are very dependent on the metal fragment, with the late transition metals showing an effect opposite from that of earlier metals.[5-10] Similarly, group 13 main-group metals exhibit less structural distortion than group 14 systems.[2,11-15] In addition, first-row metals generally show less effect than those metals of the second and third row. The nature of the ligand on the metal fragment, if any, also affects the heteroatom position with electron donors enhancing distortion toward the unique boron.[7,13] Finally, with main-group metals, the orientation of any metal-bound ligands relative to the B_3C_2 plane is found to vary from over the C–C bond in the group 13 species to over the borons in the group 14 systems.[2] On the other hand, in the group 7–9 transition-metal systems the metal fragments have rotational axes that are roughly perpendicular to the B_3C_2 plane; i.e., they exhibit symmetrical orientation of the ligand or ligands on the metal.[7]

An explanation for these effects in the icosahedral $B_9H_{11-n}C_2R_nML_x$ (M = group 10 transition metal) systems has been presented by Mingos.[5,6] Extended Hückel molecular orbital (MO) calculations showed that a four-electron antibonding interaction between the metal fragment and the carborane cage is responsible for the observed distortion. Although Eisenstein has attributed the tilting of the Ga–Me bond axis over the C_2 unit of the carborane in $MeGaC_2B_4H_6$ to a bonding interaction between the metal and the unique boron,[16] a detailed bonding study of other main-group-metal systems has not been carried out. Hence, in the following a comparison of related main-group- and transition-metal systems is presented in order to illustrate the origin of the structural distortion in a group 14 metal system.

Model Systems

The model systems chosen to study are $(2,2'\text{-bpy})SnB_4H_4(CCH_3)_2$ (bpy = bipyridine) and $(CO)_3FeB_4H_4(CCH_3)_2$. These systems were chosen because analogues of the Sn system with one or two $Si(CH_3)_3$ groups on the C_2 unit of the cage show Sn–B distances significantly shorter than Sn–C distances[13] while analogues of the Fe system have Fe–B distances slightly longer than Fe–C distances as one might normally expect.[8,9] Hence, the latter system serves as a reference or counterpoint for the investigation of the MO structure of the former. For the Sn system the crystal structure of $(2,2'\text{-bpy})SnB_4H_4C_2(SiMe_3)(Me)$[13b] provides the structural data that constitute the input for the calculations. The model cluster contains a carborane with a planar B_3C_2 face and with the Sn unit either centered above the face (Figure 1, structure **1**, Sn–C = Sn–B = 2.60 Å) or slipped 0.5 Å toward B(4) and 0.05 Å toward the carborane face (structure **2**, Sn–C = 2.77 Å, Sn–B(3,5) = 2.53 Å, Sn–B(4) = 2.36 Å). The model was symmetrized by averaging coordinates across the pseudo mirror plane with the R units anti to each other.

In order to allow direct comparison of the two metal systems,

[†] University of Notre Dame.
[‡] Southern Methodist University.

(1) Fehlner, T. P.; Housecroft, C. E. In *Molecular Structures and Energetics*; Liebman, J. F., Greenberg, A., Eds.; VCH: New York, 1986; Vol. 1, Chapter 6, pp 149–207.
(2) Hosmane, N. S.; Maguire, J. A. In *Molecular Structures and Energetics*; Liebman, J. F., Greenberg, A., Williams, R. E., Eds.; VCH: New York, 1987; Vol. 5, Chapter 14, and references therein.
(3) (a) Kennedy, J. D. *Prog. Inorg. Chem.* **1986**, *34*, 211. (b) Grimes, R. N. *Adv. Inorg. Chem. Radiochem.* **1983**, *26*, 55.
(4) Housecroft, C. E.; Wade, K. *Gazz. Chim. Ital.* **1980**, *110*, 87.
(5) Mingos, D. M. P. *J. Chem. Soc., Dalton Trans.* **1977**, 602.
(6) Mingos, D. M. P.; Forsyth, M. I.; Welch, A. J. *J. Chem. Soc., Dalton Trans.* **1978**, 1363.
(7) (a) Colquhoun, H. M.; Greenhough, T. J.; Wallbridge, M. G. H. *J. Chem. Soc., Dalton Trans.* **1985**, 761. (b) Colquhoun, H. M.; Greenhough, T. J.; Wallbridge, M. G. H. *J. Chem. Soc., Chem. Commun.* **1977**, 737. (c) Colquhoun, H. M.; Greenhough, T. J.; Wallbridge, M. G. H. *J. Chem. Soc., Chem. Commun.* **1976**, 1019.
(8) Swisher, R. G.; Sinn, E.; Grimes, R. N. *Organometallics* **1983**, *2*, 506. Maynard, R. B.; Swisher, R. G.; Grimes, R. N. *Organometallics* **1983**, *2*, 500.
(9) Brennan, J. P.; Grimes, R. N.; Schaeffer, R.; Sneddon, L. G. *Inorg. Chem.* **1973**, *12*, 2266.
(10) Pipal, J. R.; Grimes, R. N. *Inorg. Chem.* **1979**, *18*, 1936.
(11) Churchill, M. R.; Reis, A. H., Jr. *J. Chem. Soc., Dalton Trans.* **1972**, 1317.
(12) Grimes, R. N.; Rademaker, W. J.; Denniston, M. L.; Bryan, R. F.; Greene, P. T. *J. Am. Chem. Soc.* **1972**, *94*, 1865.
(13) (a) Hosmane, N. S.; de Meester, P.; Maldar, N. N.; Potts, S. B.; Chu, S. S. C.; Herber, R. H. *Organometallics* **1986**, *5*, 772. (b) Siriwardane, U.; Hosmane, N. S.; Chu, S. S. C. *Acta Crystallogr., Sect. C.: Cryst. Struct. Commun.* **1987**, *C43*, 1067. (c) Jutzi, P.; Galow, P.; Abu-Orabi, S.; Arif, A. M.; Cowley, A. H.; Norman, N. C. *Organometallics* **1987**, *6*, 1024.
(14) Hosmane, N. S.; de Meester, P.; Siriwardane, U.; Islam, M. S.; Chu, S. S. C. *J. Chem. Soc., Chem. Commun.* **1986**, 1421. Siriwardane, U.; Islam, M. S.; West, T. A.; Hosmane, N. S.; Maguire, J. A.; Cowley, A. H. *J. Am. Chem. Soc.* **1987**, *109*, 4600.
(15) Hosmane, N. S.; de Meester, P.; Siriwardane, U.; Islam, M. S.; Chu, S. S. C. *J. Am. Chem. Soc.* **1986**, *108*, 6050. Islam, M. S.; Siriwardane, U.; Hosmane, N. S.; Maguire, J. A.; de Meester, P.; Chu, S. S. C. *Organometallics* **1987**, *6*, 1936.
(16) Canadell, E.; Eisenstein, O.; Rubio, J. *Organometallics* **1984**, *3*, 759.

0020-1669/88/1327-0453$01.50/0

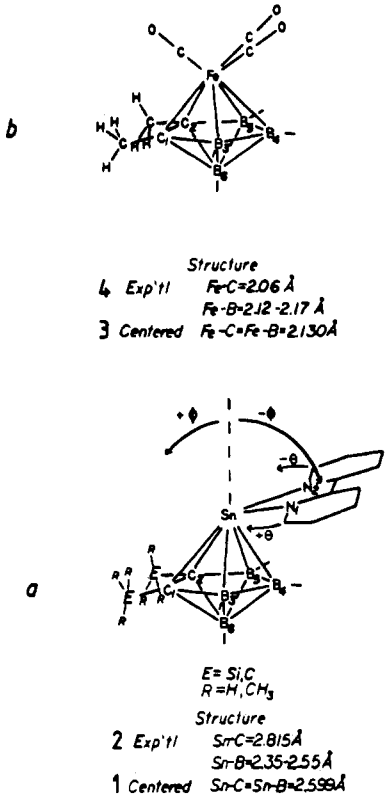

Figure 1. Model structures of (a) (2,2′-bpy)$SnB_4H_4(CCH_3)_2$ and (b) $Fe(CO)_3B_4H_4(CCH_3)_2$. The angles θ and ϕ define the orientation of the bpy ligand relative to the cage and have the values of 0 and −64° in the experimental structure.

the same carborane fragment is used for the iron system. The Fe fragment, when centered above the B_3C_2 base, is 2.13 Å from each boron and carbon. The slipped orientation is produced by taking the centered structure and moving the $Fe(CO)_3$ unit 0.10 Å toward the C–C bond (along the pseudo mirror plane) and 0.03 Å toward the B_3C_2 plane. In the slipped orientation the Fe–C(1,2) distance is 2.06 Å, Fe–B(3,5) is 2.12 Å, and Fe–B(4) is 2.17 Å. These distances are the same as those in the solid-state structure of $(C_6H_6)FeB_4H_4(CH)_2$.[8] Although $(CO)_3FeB_4H_4(CH)_2$ has been synthesized, its crystal structure has not been determined.[17] However, $(CO)_3FeB_4H_4(CH)_2$ minus the axial BH fragment, i.e., $(CO)_3FeB_3H_5(CH)_2$, has been structurally characterized in the solid state.[9] Note that the $(C_6H_6)Fe$ and $(CO)_3Fe$ units are isolobal and isoelectronic to each other. The main difference between the two is that three CO's constitute a poorer electron donor and better electron acceptor toward the metal than C_6H_6.[18] The carbonyls of the Fe unit are set mutually perpendicular to each other with Fe–C and C–O distances of 1.80 and 1.13 Å, respectively. The 3-fold axis of the $Fe(CO)_3$ unit is perpendicular to the B_3C_2 plane as shown in Figure 1b.

(2,2′-bpy)$SnB_4H_4(CSiR_3)_2$

Fragment Orbital Analysis. Structures **1** and **2** were each partitioned into two fragments. One fragment, the $[(2,2'\text{-bpy})Sn]^{2+}$ unit, has six orbitals that are of the correct symmetry and disposition to interact with the carborane fragment.[19] These orbitals (Figure 2) are as follows: 43 (s = symmetric with respect to the pseudo mirror plane) containing Sn (60%) and N (35%); 38 (a = antisymmetric with respect to the pseudo mirror plane) lying in the bpy plane containing Sn (70%) and N (25%); 37 (s) perpendicular to the bpy plane containing Sn (7%) and N (26%); 36, the LUMO (s), perpendicular to bpy localized on Sn (80%); 35, the HOMO (a), containing Sn (42%) and N (28%); and 31 (s) containing Sn (40%) and N (20%). The second fragment, $[B_4H_4(CCH_3)_2]^{2-}$, also has six orbitals of interest. These are as follows: 22 (s); 21, the LUMO (a); 20, the HOMO (s), containing 90% B and 6% C in the B_3C_2 face; 19 and 18 (a), containing 75% B and 15% C; 17 (s), containing 27% B and 68% C. Because of the anti orientation of the methyl groups, this symmetry classification is only approximate.

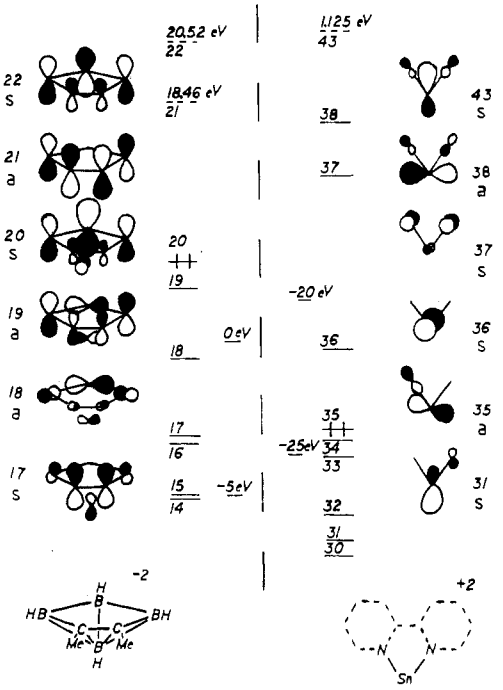

Figure 2. Fragment orbitals for $B_4H_4(CMe)_2^{2-}$ (left) and (2,2′-bpy)Sn^{2+} (right). The levels with energies specified are not to scale.

Molecular Orbitals. When the fragments are brought together to form **1** and **2**, the MO correlation diagram shown in Figure 3 results (Tables I and II, supplementary material). The energies of the fragment orbitals relative to MO energies are not arbitrarily chosen but come from the Fock matrix; i.e., these energies do not depend on the original charges assigned to the fragments. Figure 4 is a simplification of Figure 3 showing only the major changes on going from **1** to **2**. This diagram shows that there are two MO's (55, 54) whose energies are significantly affected (>0.2 eV) on going from **1** to **2**.

MO 55, the HOMO, contains an antibonding interaction that arises from symmetric Sn fragment orbitals 31, 36, and 43 (45%) and carborane orbitals 17 and 20 (45%). The schematic representation at the left of Figure 4 shows that going from **1** to **2** reduces the strong antibonding interaction between the Sn center and the carbons of the carborane and increases a weaker antibonding interaction between Sn and B(4) of the carborane. A 0.45-eV stabilization in the MO results. MO 54 has high carborane character (65–75%), and it is mainly derived from Sn orbital 38 and carborane orbitals 18 and 19. Going from **1** to **2** stabilizes MO 54 by 0.35 eV due to a more favorable interaction of the Sn orbital with the borons of the carborane face. MO's 53 and 52 experience small destabilizations (~0.2 eV) on going to **2**. The relatively small destabilization of the former is a consequence of the low amount of Sn character in the orbital.

Note that as one goes from **1** to **2** the HOMO–LUMO gap increases 0.439 eV. This results from the stabilization experienced by MO 55 as the LUMO is unaffected by the structural change. There has also been a reduction in the total energy of the system by 2.79 eV (−3854.696 → −3857.494 eV) on going to **2**. Extended

(17) Grimes, R. N. *J. Am. Chem. Soc.* **1971**, *93*, 261.
(18) (a) Elian, M.; Chen, M. M. L.; Mingos, D. M. P.; Hoffmann, R. *Inorg. Chem.* **1976**, *15*, 1148. (b) Albright, T. A.; Hofmann, P.; Hoffmann, R. *J. Am. Chem. Soc.* **1977**, *99*, 7546.
(19) The symmetry of the fragment orbitals refers to the nodal character with respect to the C_2 axis in the case of Sn(bpy) or the pseudo mirror plane of the carborane fragment. The term pseudo is added if the orbital does not fit any specific category and is used to designate the nearest symmetry class into which it does fit. Therefore, Sn orbital 35 is pseudo-σ (or pseudo-π) symmetry since the tilting of this orbital makes it neither pure σ nor π.
(20) Hoffmann, R. *Angew. Chem., Int. Ed. Engl.* **1982**, *21*, 711.

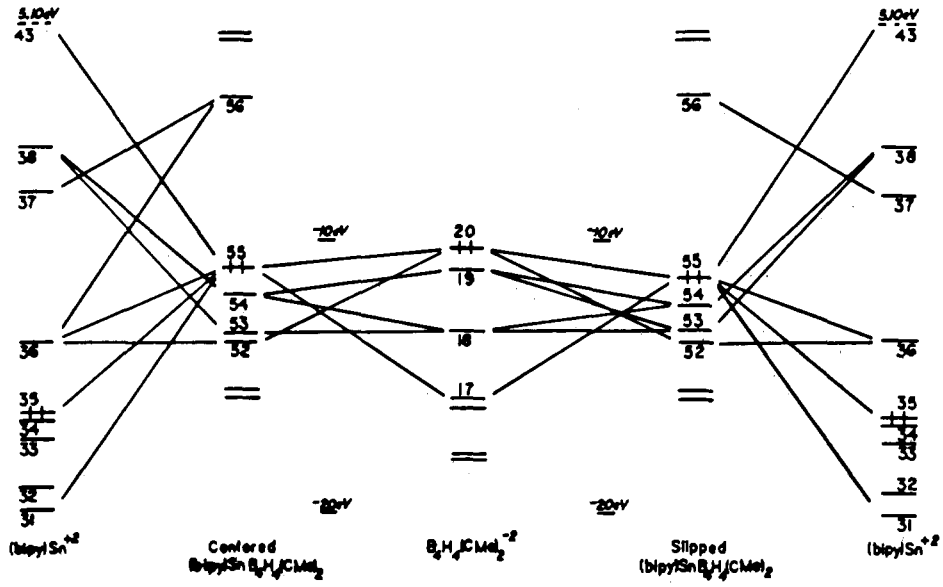

Figure 3. Molecular orbital correlation diagram for the formation of centered (**1**) and slipped (**2**) (2,2′-bpy)$SnB_4H_4(CCH_3)_2$ from $B_4H_4(CCH_3)_2^{2-}$ and $(2,2'\text{-bpy})Sn^{2+}$.

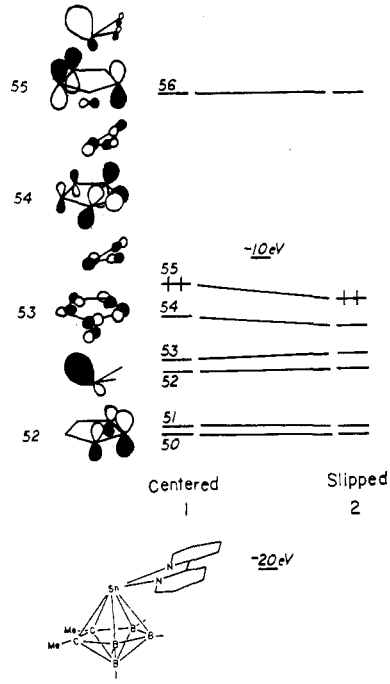

Figure 4. Orbital energy changes accompanying the distortion of (2,2′-bpy)$SnB_4H_4(CCH_3)_2$ from the centered (**1**) to the slipped (**2**) structure.

Hückel calculations also yield **2** as the structure more stable than **1**.

Overlap Populations. Overlap population is a measure of the interaction taking place between the two fragments. The values for selected fragment orbitals are listed in Tables III and IV (supplementary material) and confirm the qualitative conclusions presented above. As one goes from **1** to **2**, orbital 31 of the Sn(bpy) unit increases its overlap with carborane orbital 20 while orbital 43 loses overlap. Orbital 36 undergoes a small net loss in overlap as a gain in overlap with carborane orbital 20 is balanced against a loss in overlap with orbital 17. On the other hand, orbital 38 of the Sn unit remains essentially unchanged overall with an overlap loss to carborane orbital 18 made up by a gain in overlap to 19. For the overall structural change, there is a slight net loss in overlap population on going from **1** to **2** ($3.99 \times 10^{-1} \rightarrow 3.77 \times 10^{-1}$).

Mulliken Charges. The changes in the electron distribution within the individual fragment orbitals and the atoms with the slip distortion are examined. The Mulliken populations are listed in Tables V and VI, respectively (supplementary material). For (bpy)Sn, four orbitals show a significant (>0.005) change in Mulliken population on going to **2**. The net effect is that a small amount of charge is transferred from the carborane fragment into (bpy)Sn. This is seen in the atomic charges, which show a net charge loss by the carborane of 0.020 electron on going from **1** to **2**. This charge originates from the borons of the carborane, specifically HB(4), and largely terminates in orbital 36 of the (bpy)Sn fragment.

Summary. These results suggest that the antibonding interactions of symmetric tin fragment orbitals with corresponding carborane orbitals lying in the B_3C_2 face constitute the driving force for the adoption of the slipped structure. When the (bpy)Sn fragment is moved toward the unique boron, this antibonding interaction in the HOMO is reduced. This results in a lower total energy, a larger HOMO–LUMO gap for **2**, and a small transfer of charge from the borons of the carborane to the tin fragment.

$Fe(CO)_3B_4H_4(CMe)_2$

Fragment Orbitals. Approximate MO methods are of most value when applied in a comparative manner to related systems. Hence, in order to provide a comparison between main-group- and transition-metal carborane clusters, the $Fe(CO)_3B_4H_4(CMe)_2$ molecule, which may be considered to have a "normal" structure, has been analyzed by using the Fenske–Hall technique. In this case the fragments consist of $Fe(CO)_3^{2+}$ and $B_4H_4(CMe)_2^{2-}$. The orbitals of the latter fragment have been described above, and the fragment orbitals of $Fe(CO)_3^{2+}$ have been extensively discussed elsewhere.[18] They consist of three empty orbitals of a and e symmetry (21–19, Figure 5) and three filled "t_{2g}" orbitals (18–16). In a crude sense orbitals 21, 20, and 19 of the iron fragment correspond to orbitals 43, 38, and 36, respectively, of the tin fragment (Figures 2 and 5). Likewise, orbitals 36, 35, and 31 of the tin fragment can be identified with the iron "t_{2g}" set. This emphasizes an important difference between the fragment orbital sets. Although orbitals 35 and 31 have bonding interactions with the exo ligand as does the "t_{2g}" set of $Fe(CO)_3^{2+}$, orbital 36 is purely tin in character by symmetry and lies at significantly higher energy than orbitals 31 and 35. In the neutral tin fragment this orbital is filled and corresponds to the "lone pair". As will be seen below, this orbital constitutes the "smoking pistol" as far as the slip distortion of (bpy)$SnB_4H_4C_2(CH_3)_2$ is concerned.

Molecular Orbitals. When carborane and iron fragments are brought together to form the centered (**3**) and slipped (**4**) structures (Figure 1) of $Fe(CO)_3B_4H_4(CCH_3)_2$, the correlation diagram shown in Figure 6 results (Tables VII and VIII, sup-

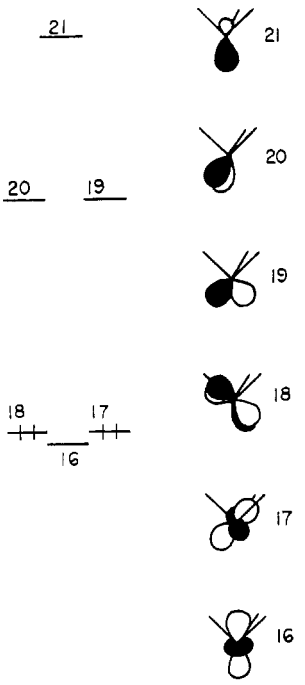

Figure 5. Fragment orbitals for $Fe(CO)_3^{2+}$. The contributions from the CO ligands are not shown.

plementary material). The interactions shown are essentially the same as those discussed earlier by Hoffmann et al.[18] A straightforward comparison of MO compositions allows the identification of the "e" set in $Fe(CO)_3B_4H_4(CCH_3)_2$ (MO's 38 plus 33 and 37) with MO's 54 plus 53 and 52, respectively, in $(bpy)SnB_4H_4(CCH_3)_2$. MO's 36–34 constitute the "t_{2g}" set. Note carefully that MO 35 of $Fe(CO)_3B_4H_4(CCH_3)_2$ is closely related to MO 55 (the HOMO) of $(bpy)SnB_4H_4(CCH_3)_2$. Although these comparisons are approximate, an examination of the MO compositions shows the close correspondence between the tin and iron systems.

When the iron capping unit is moved toward the carbons, only small changes in the energies of the filled MO's are observed. The largest change is in MO 33, which experiences a 0.19-eV stabilization in going from **3** to **4**. This should be compared to the change in the HOMO of $(bpy)SnB_4H_4(CCH_3)_2$, discussed above, which was 0.45 eV. MO 33 is CCB(3)B(5) bonding and B(4) antibonding, and the structural change enhances the bonding and reduces the antibonding interactions. Hence, structure **4** is favored over **3**.

The structural change on going from **3** to **4** results in an increase in the HOMO–LUMO gap of 0.404 eV (9.562 → 9.966 eV). In contrast to the situation with the tin compound, this is due to an increase in the energy of the LUMO on slipping rather than the stabilization of the HOMO. The former is antibonding with respect to the metal and carbons. There has also been a decrease in the total energy of the system by 1.374 eV (−1692.550 → 1693.924 eV) on going to **4**. Note that the experimentally observed distortion in $Fe(CO)_3B_4H_4(CCH_3)_2$ as well as the MO energy changes as one goes from **3** to **4** are smaller than those observed in the main-group system. Hence, the "normal" structure, **4**, for the iron cluster results from modest cluster bonding interactions whereas the "abnormal" structure, **2**, for the tin cluster is due to a large, localized, antibonding interaction that overwhelms the cluster bonding interactions still present.

Mulliken Charges. In comparison to the case for the Sn system, there is very little change in the fragment charges in going from **3** to **4**. Note that the fragments themselves are more charged than in the case of the Sn system as less of the initial fragment charge is transferred on cluster formation; i.e., in $Fe(CO)_3B_4H_4(CCH_3)_2$, the iron atom may be better represented as Fe(II) whereas in $(bpy)SnB_4H_4(CCH_3)_2$ the tin atom may be considered as Sn(0). Note also that with this choice of "oxidation" states the lower three of the six metal fragment orbitals (Figure 2 and 5) are filled in both transition- and main-group-metal fragments.

Discussion

The slipping of the capping unit along the pseudo mirror plane of the carborane fragment is clearly caused by a strong antibonding interaction between the tin fragment and the carborane base. This is dominated by an antibonding interaction between the carborane carbons and what might be considered to be the "long pair" (orbital 36) of the tin fragment in MO 55. Moving the tin fragment away from the carbons greatly stabilizes the MO by reducing this interaction.

But why does MO 55 play an important structural role in the main-group-metal compound while the corresponding MO 35 in the transition-metal cluster does not? An elementary, but not totally satisfactory, answer is that $Fe(CO)_3$ is isolobal with BH whereas (bpy)Sn is isolobal with NH; i.e., the latter has an additional electron pair. This explanation implicitly requires the partitioning of electrons in each fragment into valence and nonbonding and, in a sense, begs the question.

A better answer results from a comparison of Figures 3 and 6. The most striking difference is the large destabilizing interaction occurring between carborane fragment orbital 17 and tin orbital 36 ("lone pair") in the tin compound versus a much smaller interaction between the same carborane orbital and one of the "t_{2g}" set of the iron fragment in $Fe(CO)_3B_4H_4(CCH_3)_2$. Hence,

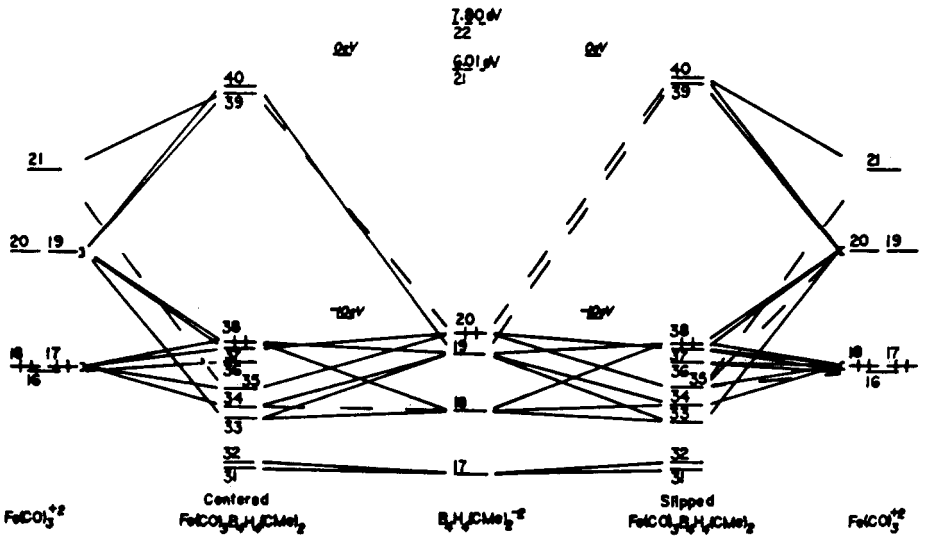

Figure 6. Molecular orbital correlation diagram for the formation of centered (**3**) and slipped (**4**) $Fe(CO)_3B_4H_4(CCH_3)_2$ from $B_4H_4(CCH_3)_2^{2-}$ and $Fe(CO)_3^{2+}$.

the difference between the two compounds is not a qualitative one but rather a difference in the magnitudes of the antibonding interactions between the nonbonding electrons of the metal fragments. In the main-group fragment the "lone pair" orbital 36, which is filled in the neutral tin fragment, is high lying and interacts strongly with the filled carborane orbital 17, which contains larger carbon character. In essence, the (bpy)Sn moiety exists in the cluster as the neutral fragment and the structure distorts to accommodate a nonbonding pair of electrons. The $(CO)_3Fe$ fragment is more cationic, and the analogous nonbonding pair is low lying and structurally inactive.

The slipped structures of the Pt(II) carboranes studied by Mingos et al.[5,6] exhibit four-electron destabilizing interactions entirely analogous to those described here. The explanations are similar as well in that the presence of an "active" pair of nonbonding electrons in the Sn and Pt clusters is considered responsible for the distorted structures. The same explanation could be provided for the slip distortion observed in the structures of (2,2′-bpy)Sn[$(Me)_2C_2B_9H_9$] and (THF)Sn[$(Me)_2C_2B_9H_9$] by Jutzi et al.[13c] A centered structure is observed in $C_2H_5AlC_2B_9H_{11}$,[11] which is consistent with the fact that the RAl fragment has no nonbonding electrons.

Since the antibonding interaction between the carborane and the metal occurs via what may be considered to be a π-symmetry orbital on the metal in the main-group system, altering the electron population in this orbital should also affect the structure. This can be done by placing a more electron donating ligand on the capping metal. The net result will be to intensify the antibonding interaction in the HOMO, which can be alleviated by further slipping the capping unit toward the unique boron of the B_3C_2 face. Such an explanation has been used by Colquhoun et al. to explain the different structures of 3-L_2-3,1,2-$PdC_2B_9H_{11}$ systems.[7] Here there is a larger displacement toward the borons when $L_2 = Me_2N(CH_2)_2NMe_2$, an electron donor, than when $L = PMe_3$, a π acceptor.

A second way to increase the electron population of the critical metal orbital is to increase the donation from the carborane fragment. As one goes down a column of the periodic table, the effective nuclear charge of the metal center is increased, thereby stabilizing the metal orbitals relative to those of the carborane. In the group 14 main-group-metal and d^8 transition-metal systems, this will increase the antibonding interaction between the metal and the carborane carbons and therefore result in an increase in slippage. Note that as one goes from **1** to **2** there is an increase in the Mulliken populations of both Sn fragment orbital 36 ("lone pair") and carborane fragment orbital 17 (high CC character) (Figure 2, Table V). For the transition-metal systems, going from Pd to Pt (with the same capping ligand and carborane) results in a 0.22-Å increase in C–M distance.[7]

The final point to be made deals with the orientation of the capping ligand. For the tin system, the tilting of the bpy ligand is the result of the antibonding interaction taking place in the HOMO, MO 55. A major contributor to this MO is fragment orbital 36, which is derived from a tin p orbital perpendicular to the bpy plane (Figure 2). In order to reduce the antibonding interaction, the (bpy)Sn unit tilts away from the SnC_2 face. This explanation is qualitatively the same as that used by Cowley[21] and Eisenstein[16,22] to describe the bent structures seen in main-group sandwich compounds. Further, since it is an antibonding effect, the tilting of the capping ligand should increase with increased antibonding, i.e. with increased slipping away from the carbons. Therefore, it would be expected that going down a periodic series will increase not only the slipping but also the tilting as the "lone pair" orbital becomes more important. This prediction has yet to be proven for the main-group carborane species, but for sandwich compounds of the type $(C_5H_5)_2M$ (M = Sn, Pb), the tilting between the Cp rings is larger for Pb than for Sn.[23] However, the tilting of the MeGa fragment in $MeGaC_2B_4H_6$ over the carbons reflects the bonding interaction between the metal and the unique boron.[16] In the absence of an "active lone pair", the cluster bonding interactions are revealed in the exo-ligand orientation.

Calculations

Preliminary calculations were carried out by using the extended Hückel method with parameters obtained as described in earlier work.[24] The principal calculations employed the nonparameterized Fenske–Hall technique,[25] and most of the basis functions used were the same as used earlier.[26] The Sn functions were obtained from M. B. Hall.

Acknowledgment. This work was supported by grants from the National Science Foundation and the donors of the Petroleum Research Fund, administered by the American Chemical Society. We thank the Computing Center of the University of Notre Dame for providing computational time and Professor M. B. Hall for the tin basis functions.

Registry No. (2,2′-bpy)$SnB_4(CH_3)_2$, 112021-81-5; $(CO)_3FeB_4H_4(CH_3)_2$, 112021-82-6.

Supplementary Material Available: Tables I–XII, showing MO compositions, fragment–fragment overlap populations, fragment charges, and atomic charges for (bpy)$SnB_4H_4(CCH_3)_2$ and $Fe(CO)_3B_4H_4(CCH_3)_2$ in the centered and slipped structures (7 pages). Ordering information is given on any current masthead page.

(21) Baxter, S. G.; Cowley, A. H.; Lasch, J. G.; Lattman, M.; Sharum, W. P.; Stewart, C. A. *J. Am. Chem. Soc.* **1982**, *104*, 4064.
(22) Eisenstein, O.; Canadell, E.; Thanh, B. T. *Nouv. J. Chim.* **1986**, *10*, 421.
(23) Atwood, J. L.; Hunter, W. E.; Cowley, A. H.; Jones, R. A.; Stewart, C. A. *J. Chem. Soc., Chem. Commun.* **1981**, 925.
(24) Hoffmann, R. *J. Chem. Phys.* **1963**, *39*, 1397. Bernstein, J.; Hoffmann, R. *Inorg. Chem.* **1984**, *24*, 4100. Burdett, J. K.; Canadell, E.; Miller, G. J. *J. Am. Chem. Soc.* **1986**, *108*, 6561. Andersen, E. L.; DeKock, R. L.; Fehlner, T. P. *Inorg. Chem.* **1981**, *20*, 3291.
(25) Hall, M. B.; Fenske, R. F. *Inorg. Chem.* **1972**, *11*, 768. Hall, M. B. Ph.D. Thesis, University of Wisconsin, Madison, WI, 1971. Fenske, R. F. *Pure Appl. Chem.* **1971**, *27*, 61.
(26) Fehlner, T. P.; Housecroft, C. E. *Organometallics* **1984**, *3*, 764.